New clinical forms of hereditary apoA-I amyloidosis entail both glomerular and retinal amyloidosis

Magali Colombat, Jean-Claude Aldigier, Pierre-Raphael Rothschild, Vincent Javaugue, Estelle Desport, Thierry Frouget, Jean-Michel Goujon, Nathalie Rioux-Leclercq, Nathalie Quellard, Jean Philippe Rerolle, et al.

[QUERY TO AUTHOR: title and abstract rewritten by Editorial Office – not subject to change]

New clinical forms of hereditary apoA-I amyloidosis entail both glomerular and retinal amyloidosis.

Magali Colombat[1], Jean-Claude Aldigier[2], Pierre-Raphael Rothschild[3], Vincent Javaugue[4], Estelle Desport[4], Thierry Frouget[5], Jean-Michel Goujon[6], Nathalie Rioux-Leclercq[7], Nathalie Quellard[6], Jean Philippe Rerolle[2], François Paraf[8], Caroline Beugnet[9], Aurélien Tiple[10], Antoine Durrbach[11], Didier Samuel[12], Antoine Brézin[3], Frank Bridoux[4], and Sophie Valleix[9]

[1]Service d'Anatomopathologie, Institut Universitaire du Cancer Toulouse Oncopole, CHU Toulouse, Toulouse, France; [2]Service de Néphrologie et de transplantation rénale, CHU Dupuytren, Limoges, France; [3]Service d'Ophtalmologie, OphtalmoPôle, Hôpital Cochin, Université de Paris, Assistance Publique-Hôpitaux de Paris, AP-HP, Paris, France; [4]Service de Néphrologie, hémodialyse et transplantation rénale, CHU Poitiers, Poitiers, France; [5]Service de Néphrologie, CHU Pontchaillou, Rennes, France; [6]Service d'Anatomie Pathologique, Unité de microscopie électronique, CHU La Miletrie, Centre de Référence National Amylose AL et autres maladies de dépôts d'immunoglobulines monoclonales, Université de Poitiers, Poitiers, France; [7]Laboratoire d'Anatomopathologie, CHU Pontchaillou, Rennes, France; [8]Laboratoire d'anatomopathologie CHU Dupuytren, Limoges, France; [9]Laboratoire de Génétique Moléculaire, Fédération de Génétique, Hôpital Necker-Enfants Malades, Université de Paris, Assistance Publique-Hôpitaux de Paris, AP-HP, Paris, France; [10]Service de Néphrologie et Transplantation, Centre Hospitalier Jacques Lacarin de Vichy, Vichy, France; [11]Service de Néphrologie, Hôpital de Bicêtre, Assistance Publique-Hôpitaux de Paris, AP-HP, Le Kremlin-Bicêtre, France; [12]Centre hépato-biliare, Hôpital Paul Brousse, Assistance Publique Hôpitaux de Paris, AP-HP, Villejuif, France.

Correspondence: Sophie Valleix, Laboratoire de Génétique Moléculaire, Fédération de Génétique, Hôpital Necker-Enfants Malades, 147 rue de Sèvres, 75015 Paris, France. E-mail : sophie.valleix@aphp.fr

KEYWORDS: AApoAI amyloidosis, glomerular amyloidosis, amyloidogenic cysteine-frameshift apoA-I variant, retinal amyloidosis, combined hepatorenal transplantation

Running title: Glomerular and retinal amyloidosis in AApoAI

ABSTRACT

Apolipoprotein A1 amyloidosis (ApoAI) results from specific mutations in the *APOA1* gene causing abnormal accumulation of amyloid fibrils in diverse tissues. The kidney is a prominent target tissue in ApoAI amyloidosis with a remarkable selectivity for the renal medulla. Here, we investigated six French families with ApoAI Glu34Lys, p.His179Profs*47, and a novel p.Thr185Alafs*41 variant revealing unprecedented clinical association of a glomerular with a retinal disease. Comprehensive clinicopathological, molecular and proteomics studies of numerous affected tissues ensured the correlation between clinical manifestations, including novel unrecognized phenotypes, and apoA-I amyloid deposition. These ophthalmic manifestations stemmed from apoA-I amyloid deposition, highlighting that the retina is a previously unrecognized tissue affected by ApoAI amyloidosis. Our study provides the first molecular evidence that a significant fraction of ApoAI amyloidosis cases with no family history result from spontaneous neomutations rather than variable disease penetrance. Finally, a successful hepatorenal transplantation resulted in a life- and vision-saving measure for a 32-year-old man with a hitherto unreported severe ApoAI amyloidosis caused by the very rare Glu34Lys variant. Our findings reveal new modes of occurrence and expand the clinical spectrum of ApoAI amyloidosis. The awareness of glomerular and ocular manifestations in ApoAI amyloidosis should enable earlier diagnosis and avoid misdiagnosis with other forms of renal amyloidosis. Thus, documented apoA-I amyloid deposition in the retina offers new biological information about this disease and may change organ transplantation practice to reduce retinal damage in patients with ApoAI amyloidosis.

INTRODUCTION

Apolipoprotein A-I (apoA-I) is the major constituent of plasma high-density lipoprotein (HDL) particles that removes excess cholesterol from peripheral cells.[1] Numerous naturally occurring *APOA1* mutations are associated with increased risk of atherosclerosis and familial coronary heart disease, while others become amyloidogenic and cause hereditary apoA-I amyloidosis (AApoAI) in humans.[2] AApoAI is a rare form of autosomal dominant disease wherein specific mutations in the *APOA1* gene cause abnormal accumulation of predominantly N-terminal fragments of the variant protein as amyloid fibrils in diverse tissues.[3,4] The exact molecular events whereby *APOA1* mutations trigger amyloid are not fully defined, but structural destabilization of the N-terminal helix bundle domain is likely the pathogenic mechanism of all amyloidogenic apoA-I variants.[5,6] More recently, Gursky's team proposed that a localized structural change causing abnormal solvent exposure of the major N-terminal amyloid hotspot in residues L11-L22 of apoA-I, might be an early trigger of protein misfolding in amyloid.[7]
Human apoA-I is a 243-residue polypeptide that folds into two structural domains, comprising a globular N-terminal domain (residues 1-184) and a more flexible C-terminal domain (residues 190-243). The 20 *APOA1* mutations reported to date are clustered in two distinct regions of the N-terminal domain (residues 1-90 and 154-178) causing amyloid deposition of the N-terminal 80-100-residues fragments of the mutated apoA-I mainly in kidney, liver and spleen.[8] Remarkably, AApoAI is clinically highy variable and can present as an aggressive disease with early onset and widespread systemic amyloid deposition leading to a fatal outcome around the fifth decade of life; alternatively, AApoAI may have a mild phenotype restricted to amyloid in only one organ.[9,10] Also, AApoAI can present with a typical autosomal dominant inheritance or with a sporadic presentation with no family history[10]; whether these sporadic AApoAI cases reflect variable penetrance of the disease or result from *de novo APOA1* mutations is unknown. Therefore, these sporadic cases can frequently be misdiagnosed as AL or AA amyloidosis, the most prevalent types of acquired amyloidosis with renal involvement.[11] In regards to renal involvement, AApoAI is typically characterized by chronic tubule-interstitial nephritis that manifests as slowly progressive renal failure with no proteinuria, and renal amyloid deposits restricted to the tubules, vessels and interstitium of the inner medulla, sparing glomeruli.[12-14] While these AApoAI renal

pathological characteristics were described for numerous patients with Pro75Leu and Gly26Arg variants, very rare AApoAI cases manifesting as nephrotic syndrome and renal dysfunction due to amyloid deposits at the glomerular level have been reported.[10,15,16] But, due to a relatively limited number of clinico-pathogenic studies of AApoAI cases with unusual renal presentation, further investigations were needed to confirm whether AApoAI may have distinct renal characteristics depending on mutation type.

We present a comprehensive clinicopathological, molecular and proteomics study of six unrelated French AApoAI families associated with Glu34Lys (2 kindreds), p.His179Profs*47 (3 kindreds), and a novel p.Thr185Alafs*41 variant in one kindred, revealing novel systemic clinical presentations, including a glomerular and a retinal amyloid disease.

RESULTS

Clinical investigations

Family A: A 23 year-old man (proband III.3 in Figure 1a) presented with an eight-year history of hypertension, proteinuria (4.5g/24h), and renal dysfunction (serum creatinine at 2.1 mg/dl) as starting symptoms, followed by infertility. Ultrasound of the abdomen revealed hepatomegaly and splenomegaly. Nerve conduction studies were normal and cardiac investigations did not reveal any evidence of cardiomyopathy. There was no history of paraesthesia or autonomic symptoms, and no evidence of a plasma cell dyscrasia. Baseline tests showed abnormal renal and liver functions (alkaline phosphatases: 571 U/l, aspartate aminotransferase: 137U/l, alanine aminotransferase: 88U/l, gamma-glutamyltransferase: 994U/l). Serum levels of triglycerides were 1.81 g/l, HDL-cholesterol 0.32 g/l, and LDL-cholesterol 1.22 g/l. Endocrine testing demonstrated hypergonadotrophic hypogonadism with a dramatic drop in plasma concentrations of 17β-estradiol, testosterone, and dihydrotestosterone, and increased plasma concentrations of follicle-stimulating hormone and luteinizing hormone. The proband's mother (II.3) had developed nephrotic syndrome and renal insufficiency at age 28, and had biopsy-proven amyloid in the glomerular compartment, liver and heart. Because of absence of family history of amyloidosis, a coincidentally increased serum level of free immunoglobulin light chain, and inconclusive immunohistochemistry, this proband's mother (II.3) was diagnosed with light-chain amyloidosis (AL), and received autologous bone marrow stem cell transplant with no improvement in renal function, and finally died of infection.

Family B: A 39 year-old man (proband II.4 in Figure 1b) presented with a 20-year history of hypertension, infertility with severely decreased testosterone levels, chronic diarrhea, and a persistent subnephrotic range of proteinuria (2.01 g/24 h) associated with renal and liver dysfunction. Neurological examination was normal, but electromyography revealed mild axonal sensory motor polyneuropathy. Cardiac amyloid infiltration was suggested by echocardiogram demonstrating a 15-mm interventricular wall thickness. Free immunoglobulin light chains were within a normal range, and immunofixation of serum or urine showed no evidence of monoclonal gammopathy. Tests of liver function showed high serum alkaline phosphatase (854 UI/l), high gamma-glutamyl transpeptidase (594 UI/L), and moderately increased aspartate aminotransferase (69 U/L) and alanine aminotransferase (63 U/L). Abdominal

ultrasound revealed hepatomegaly and splenomegaly. Although all tests for an underlying inflammatory or infectious condition were negative, the diagnosis of amyloid A amyloidosis secondary to urogenital tuberculosis was suspected on the basis of widespread abdomino-pelvic calcifications (Figure 1c), and absence of family history of amyloidosis. Despite antituberculosis treatment, the renal and liver functions gradually deteriorated, with proteinuria reaching 8g/24 h, and the development of bleeding esophageal varices and hepatic encephalopathy. Ultimately, this patient died from renal and liver failure at age 49.

Family C: A 58 year-old woman of French ancestry was referred for recently discovered proteinuria (proband III.3 in Figure 2c). Her father died from chronic renal failure of unknown origin. On admission, physical examination revealed diffuse lower limb edema. Blood pressure was 144/88 mmHg. Skin, abdominal, cardiac and neurological investigations were normal. Biological tests showed nephrotic syndrome (total protein 59 g/l, albumin 22 g/l, 24 proteinuria 10.4 g/24h. Renal function was normal with urea of 5.7 mmol/l, serum creatinine of 64 µmol/l, and glomerular filtration rate (calculated using the simplified MDRD equation) of 88 ml/min/1.73m^2. Full blood count, coagulation and liver function tests were normal with normal CRP and serum SAA levels, and there was no evidence of a plasma cell dyscrasia. Serum levels of triglycerides were 1.4 g/l, apoA-I 0.83 g/l, HDL-cholesterol 0.28 g/l, total cholesterol 2.69 g/l, LDL cholesterol 2.91g/l. Kidney biopsy revealed amyloid in glomeruli. Kidney biopsy revealed amyloid in glomeruli.

Family D: A 62-year old French male (proband II.1 in Figure 2d) with no family history of renal or liver disease presented with edema, hypertension and was discovered to have nephrotic proteinuria in the range of 10g/24h and stage 3 chronic kidney disease. A renal biopsy was positive for amyloid in the glomerular compartment. Cardiac investigations did not suggest amyloid cardiomyopathy, and neurologic examination was normal. A workup was negative for monoclonal gammapathy. Full blood count, coagulation and liver function tests were normal with normal CRP and serum SAA levels.

Family E: The proband was a 65-year old French male (individual II.1 in Figure 2c) presenting with nephrotic proteinuria (serum creatinine 85 µmol/l, proteinuria 6,5 g/24H) of unknown cause. He had no oedema and there was no clinical evidence of peripheral or autonomic neuropathy, except a personal history of carpal tunnel syndrome. Cardiac biologic markers were slightly elevated but cardiac MRI showed no

features of amyloid deposition. There was no evidence of monoclonal gammapathy on immunofixation of serum or urine, and there was no family history of renal disease. All baseline blood biochemistry tests were within normal limits. Plasma triglyceride levels were 1.55 g/l, HDL-cholesterol levels 0.26 g/l, and LDL-cholesterol levels 0.9 g/l. A renal biopsy detected amyloid in the glomerular compartment.

Family F: A 52-year old French man was referred for nephrotic syndrome (proband II.1 in Figure 3.a). His personal and family history was unremarkable. On admission, blood pressure was 110/70 mmHg and physical examination revealed marked lower limb oedema without extrarenal manifestations. Biological tests showed: proteinuria 3.5 g/24h, serum albumin 28 g/l, serum creatinine 66 µmol/l with estimated glomerular filtration rate (MDRD equation) 110 ml/min/1.73m^2. Liver function tests showed: ASAT 16 UI/l, ALAT 11 UI/l, alkaline phosphatases 50 UI/l, and gamma GT 28 UI/l. Full blood count was normal. Serum CRP level was <1 mg/l, with SAA <3 mg/l. Serum and urine immunofixation did not show evidence of paraprotein. Serum free light chains were within normal ranges (kappa 21 mg/l, lambda 13 mg/l, kappa/lambda ratio 1.6). Ultrasound examination of the abdomen was unremarkable. Electrocardiography and cardiac ultrasound scan were normal (septum thickness 72 mm). Serum levels of NT-proBNP (25 ng/l) and troponin T (<0.013 µg/l) were normal. Plasma apoA-I levels were 0.71 g/l, triglyceride 3.62 g/l, and HDL-cholesterol was 0.22 g/l. Salivary glands and abdominal fat biopsies were negative for amyloidosis. A kidney biopsy revealed segmental Congo red-positive amyloid deposits restricted to the glomeruli.

AApoAI is associated with a massive choroidal amyloid angiopathy

Ophthalmological manifestations were first discovered in patients with Glu34Lys, who presented with a history of unexplained transient episodes of bilateral visual loss and metamorphopsia in their 30s or 40s. Fundus examination showed bilateral ovoid yellowish deposits at the midperipheral retina in the form of linear streaks and around the optic nerve head, but no vitreous opacities were observed (Figure 4a). Fundus autofluorescence (FAF) revealed bilateral areas of autohypofluorescence in the peripapillary region with surrounding hyperautofluorescence with an hyperautofluorescent gravitational track from the optic disc to the inferior midperipheral retina (Figure 4b). Fluorescein angiography (FA) revealed bilateral staining around the optic discs, which was particularly prominent in the nasal

peripapillary area, which might be suggestive of peripapillary infiltration by amyloid deposits (Figure 4c). The most striking lesions were discovered at indocyanine Green angiography (ICGA) which revealed hyperfluorescent streaks radiating from the optic discs and following the course of choroidal vessels with a diffuse "firework" pattern associated with diffuse hypocyanescent dark lesions of variable size (Figures 4d-e). Optical coherence tomography (OCT) showed bilateral peripapillary ring of shallow serous retinal detachments along with subretinal fluid accumulation at different sites, an irregular aspect of the RPE layer, and numerous reflective spots between RPE and the neuroretina that may represent intraretinal amyloid deposits (Figure 4f). Proband II.4 from family B progressively developed recurrent serous retinal and choroidal detachments with massive cystoid macular edema leading to end-stage blindness (Figure 4g). Further ophthalmological investigations of AApoAI patients with p.His179Profs*47 and p.Thr185Alafs variants, except proband from family E who denied investigations, identified similar *in vivo* choroidal vascular lesions at late-phase ICGA than those observed for Glu34Lys carriers. Therefore, choroidal amyloid angiopathy should be considered in AApoAI patients, and ICGA is highly beneficial to detect this subclinically "occult" amyloid angiopathy at the earliest possible stage of the disease.

Genetic analyses

In family A, *APOA1* sequence analysis from proband III.3 revealed a heterozygous single-base substitution in exon 3 (c.172G>A) resulting in Glu to Lys substitution at amino acid position 34 of the mature protein, Glu34Lys (p.Glu58Lys; p.E58K) (http://www.amyloidosismutations.com) (Figure 1d*)*. While the proband's mother (II.3) was dead and could not be tested, DNA from seven clinically asymptomatic family members was genotyped. Glu34Lys was not detected in the proband's sister (III.4), father (II.4), aunt (II.2), and first cousins (III.1 and III.2) from the maternal side. Importantly, Glu34Lys was absent from the DNA of both proband's maternal grandparents (I.1 and I.2), suggesting strongly that Glu34Lys emerged *de novo* in the proband's mother (II.3) (Figure 1a). In family B, Glu34Lys was also identified in proband II.4 in heterozygous state, but was absent from DNA samples of both his parents (I.1 and I.2), and in all asymptomatic family members (II.1, II.2, and II.3), further suggesting that Glu34Lys also arose *de novo* in this second kindred (Figure 1b). In families C, D, and E genetic analyses from probands revealed heterozygosity in exon 4 for a same GC-

dinucleotide duplication at position c.532_533 (c.532_533dup) within the GC-tandem repeat sequence present from nucleotide position 524 to 533 of the c.DNA sequence of the *APOA1* gene (Figure 2d). The observed DNA changes would lead to a shift in the reading frame from residue Ala154 of the mature wild-type amino acid sequence and cause premature termination 47 amino acids downstream, annoted as Ala154Profs*47; p.His179Profs*47 (http://www.amyloidosismutations.com). Parents from families D and E, but not family C, were available for clinical examination and genetic evaluation. The data showed that the c.532_533dup; p.His179Profs*47 variant was absent in both proband's parents of families D and E, who were clinically asymptomatic, showing that c.532_533dup; p.His179Profs*47 variant arose *de novo* in both probands (Figures 2b-c). In family F, a GC-dinucleotide duplication (c.552_553dup) in heterozygous state was identified in the proband II.1, predicting a shift in the reading frame from residue Thr161 of the mature wild-type amino acid sequence with premature termination 41 amino acids downstream: Thr161Alafs*41; p.Thr185Alafs*41 (Figure 3b). This novel frameshift variant was not detected nor in the proband's parents (I.1 and I.2) neither in his two sisters (II.2 and II.3), suggesting that it occurred *de novo* in proband (II.1) of this family (Figure 3a). There was no family history of amyloidosis, and the proband's parents (I.1 and I.2) were clinically unaffected.

Histopathological features and amyloid typing

Kidney biopsies were available for a total of seven AApoAI probands, and all cases showed deposition of amyloidosis in glomeruli. The p.Thr185Alafs*41 variant is novel and the p.His179Profs*47 variant has been reported once without detailed anatomopathological data[15]. Pathological renal characteristics associated with p.Thr185Alafs*41 and p.His179Profs*47 were similar, and revealed diffuse thickening of glomerular capillary walls due to deposition of amorphous eosinophilic material that was identified as amyloid by green birefringence in cross polarized light microscopy after staining with Congo red (Figure 5a-b). Amyloid deposits displayed a predominant membranous distribution, with less pronounced involvement of the mesangial areas. Examination of silver-stained sections showed that the glomerular amyloid deposits were closely associated with unusual changes in the capillary walls. These lesions were characterized by irregularities, sometimes focal disappearance or duplication of the glomerular basement membranes (Figure 5c). Extensive interstitial fibrosis was

observed, but tubule-interstitial areas and intra-renal vessels contained no amyloid. Transmission electron microscopy revealed that glomerular capillary walls were massively invaded by non-branched, randomly arranged fibrils that had all the characteristics of amyloid (Figure 5d). While fibrils were observed in the mesangial and sub-endothelial areas, they were mainly sub-epithelial and sometimes traversed the glomerular basement membrane to penetrate the urinary space (Figure 5e). The *lamina densa* of the glomerular basement membrane was markedly thin and sometimes focally disrupted in the areas of massive amyloid deposition (Figure 5f). Electron microcopy demonstrated that amyloid fibrils were found in the glomerular structures only, and were absent in tubule-interstitial areas (Figure 5g). Glomerular amyloid deposits were stained strongly positive by indirect immunofluorescence with a monoclonal anti-apoA-I antibody, showing a membranous staining pattern (Figure 5h) that was congruous with Congo red staining. Immunotransmission electron microscopy (immuno-TEM) of kidney sections further demonstrated the prominent sub-epithelial distribution of extracellular glomerular amyloid fibrils that were decorated positively by gold particles linked to the apoA-I antibody (Figure 5i). Again, immuno-TEM did not detect tiny amyloid fibril deposits in tubule-interstitial, not detectable by CR staining. For the Glu34Lys variant, renal histopathological findings detected amyloid in the glomerular compartment within mesangial areas but again with a strong predilection for GBM with spicule formation (Figure 6a-b). Jones silver stain showed glomerular expansion by an amorphous, pale, « cotton candy » silver negative material that corresponds to amyloid deposits (Figure 6c-d). These deposits were located within the mesangium and the capillary loops. The capillary loops appeared thickened due to subendothelial and subepithelial deposition associated with presence of spicules along the GBM (Figure 6c-d). Amyloid was also detected in the liver (Figure 6e), heart (Figure 6f), and testes that were invaded by massive deposits spreading thorought the interstitial tissue associated with a severely reduced number of seminiferous tubules without spermatogenesis (Figure 7a-b). A tiny retinal specimen was obtained during surgery for massive serous retinal detachment occurred in proband II.4 of family B; histological analysis revealed the presence of several typical amyloid deposits with apple-green birefringence upon Congo red staining (Figure 7c-f). To ensure that all clinical systemic manifestations associated with Glu34Lys, notably those unrecognized until now, were correlated with amyloid deposition in affected organs, laser

microdissection (LMD) and liquid chromatography tandem mass spectrometry (LC-MS/MS) was used to identify the fibrillar protein in amyloid. Proteomic analysis of microdissected Congo-red-positive deposits was performed using testicular and liver biopsies from proband III.3 of family A, cardiac biopsy from proband II.3 of family A, and renal and retinal specimen from proband II.4 of family B (Figures 8a-b, 9a-b, and 10a). The results revealed the presence of large numbers of apoA-I protein spectra from all these affected organs, along with apoE and SAP, which are the universal "amyloid signature" proteins, and excluded the presence of other amyloid precursor proteins. Importantly, sequence coverage of the deposited apoA-I protein showed the presence of the apoA-I tryptic peptide containing the mutated Lys34, demonstrating amyloid deposition of Glu34Lys variant in all affected tissues (Figure 10b).

Favourable outcome of combined hepatorenal transplantation for a young Glu34Lys AApoAI patient

After a multidisciplinary discussion that considered the extensive multisystem nature and the severity of the amyloid disease in patient II.4 from family B with fatal encephalopathy and blindness, a combined hepatorenal transplantation was proposed to proband III.3 from family A at age 32. The rationale for this dual transplantation was not only to offer a survival advantage by restoring normal liver and renal function, but also to slow the retinal damage, since the amyloid in choroidal vessels probably originated from hepatic production of variant apoA-I. No post-operative complications were observed, and there were no acute rejection episodes of either transplant. Renal and liver functions rapidly recovered, and the patient reported a remarkable improvement of his general well-being and started exercising six months after the dual transplantation. Evaluation at four years post-transplantation, both grafts were functioning very well, and no amyloid was not detected on a kidney transplant biopsy. The patient is currently asymptomatic and did not develop any cardiac or neuropathic manifestations. Laboratory tests showed normal hepatic and renal functions with no proteinuria, and serum triglyceride levels were 1.24 g/l, HDL-cholesterol 0.38 g/l, LDL-cholesterol 1.41 g/l, and apoA-1 level was 0.95 g/l, six months after transplantation. More importantly, the patient showed significant improvement of his ocular symptoms, and did not experience any retinal detachments. The excellent clinical outcome

highlights the feasibility and effectiveness of combined transplantation in young AApoAI adults.

DISCUSSION

Renal involvement is a prominent common feature in different forms of acquired and hereditary amyloidosis[17], notably in fibrinogen A alpha chain (AFib),[18] apolipoprotein A2 (AApoAII),[19] lysozyme (ALyz),[20] gelsolin (AGel),[21,22] apolipoprotein C3 (AApoCIII),[23] apolipoprotein C2 (AApoCII),[24] and apolipoprotein A1 (AApoAI) amyloidosis[9]. Amyloid deposition can be seen in any of the parenchymal compartments, including glomeruli, tubulointerstitium, and vasculature, but glomeruli remain the most commonly affected structure. Clinical and histological features of renal amyloidosis vary according to the type, but for a same type of amyloidosis, the renal characteristics are usually relatively uniform. For example, AFib is typically characterized by massive amyloid in glomeruli, while AApoAI is typically characterized by large amyloid deposits restricted to the medulla, completely sparing the glomeruli.[12-14] However, AApoAI has been unexpectedly associated with a distinctive renal presentation with amyloid inside glomeruli only, in a small fraction of cases.[10,15,16] This study reports six AApoAI kindreds with Glu34Lys, p.His179Profs*47 and a novel amyloidogenic p.Thr185Alafs frameshift apoA-I variant, all presenting a nephrotic-range proteinuria and CKD. The Glu34Lys and p.His179Profs*47 are very rare apoA-I variants previously reported in two unrelated sporadic AApoAI cases[10,15] and in a single AApoAI case[16] respectively, associated with proteinuria and CKD with amyloid deposits in glomeruli.[12-14] Here, seven additional AApoAI kidney biopsies also detected Congo red–positive amyloid deposits inside the glomeruli, that were shown, in each case, to contain the corresponding apoA-I variant as the amyloid fibril protein by a combination of immunofluorescence, immuno-electron microscopy, or proteomic analysis. Moreover, electron microscopy of tubules did not reveal amyloid, supporting the glomerular restriction of amyloid. The reported histologic findings in glomeruli associated with Glu34Lys, p.His179Profs*47 and p.Thr185Alafs variants showed a strong predilection of amyloid for GBM with spicule formation, as it is observed for AL type amyloidosis. Therefore, the renal anatomopathological patterns of amyloid differ in AApoAI depending on the mutation type, and can be characterized by either a predominant medullar or a glomerular pattern, rendering the diagnosis of AApoAI very challenging.[10,16] Therefore, in addition to AFib and AGel hereditary amyloidosis, AApoAI must also be suspected in case of predominant glomerular involvement.

This is the first study reporting a glomerular disease in AApoAI patients which was accompanied by visual impairment explained by a choroidal angiopathy as demonstrated, here, for the first time, *in vivo,* using ICG angiography. Ocular manifestations are described in hereditary transthyretin amyloidosis (ATTR),[25-27] but are uncommon in this form of amyloidosis, and no causal link between retinal amyloidosis and AApoAI has been established to date. Here, a retinal specimen from one Glu34Lys-carrier allowed us to directly identify amyloid deposits definitively confirming the correlation between the clinical ocular symptoms and amyloid deposition in the corresponding affected tissue. LC-MS/MS analysis of retinal deposits showed the presence of a large numbers of apoA-I protein spectra along with SAP and apoE, and detected Glu34Lys variant. This complete anatomopathological concordance provides the first conclusive evidence of choroidal vascular lesions in eyes with AApoAI due to amyloid deposition of apoA-I. Therefore, choroidal amyloid angiopathy should be considered in AApoAI patients, and ICG angiography is highly beneficial to detect clinically silent choroidal/retinal involvement at the earliest possible stage of the disease. This new risk of vision loss is likely to change organ transplantation practice in AApoAI by encouraging combined hepatorenal transplantation, as previously proposed when there is clinically significant impairment in nontranposable organs.[28,29] Although apoA-I has two sources of production, the liver and the small intestine, we report here the favourable outcome of combined hepatorenal transplantation performed in a 32-year-old man with Glu34Lys, as judged by the 5-year graft survival with no amyloid recurrence on the renal graft and the remarkable symptomatic benefits.

We also show that Glu34Lys variant causes early-onset male infertility due to massive amyloid deposition in testes. A similar clinical presentation was previously reported for a large number of Leu75Pro AApoAI carriers.[30] Therefore, testicular involvement in AApoAI might be more common than previously thought, leading to early-onset decline in male reproductive fitness. This strong negative selection factor is expected to reduce the number of apoA-I mutant alleles in the general population, unless the new mutational rate is high.[31] Here, a family history of renal disease or amyloidosis was absent in five AApoAI kindreds with the available evidence here, for the first time, that this was due to *de novo* mutations rather than reduced penetrance, as it is observed in Aα-chain amyloidosis (AFib) associated with p.Glu545Val (E526V) variant.[32] This new knowledge will help to improve timely diagnosis of AApoAI in sporadic cases

of systemic amyloidosis and to avoid misdiagnosis as AL or AA amyloidosis, the most common forms of acquired systemic amyloidosis.[11]

The reasons why some apoA-I variants preferentially accumulate in the renal medulla while others in the glomerular compartment remain unknown. The mutations reported here, include one "inside" missense and two "outside" frameshift mutations, that drastically differ in their amino acid changes emphazing that additional factors, other than the mutation alone, are involved in preferential tissue deposition of apoA-I fibrils. Most AApoAI patients reported to date, present with a moderate hypoalphalipoproteinemia, and it has been shown that it can be the consequence of an impaired secretion and/or an accelerated metabolism of apoA-I,[33] but HDL/apoA-I metabolism associated with AApoAI, remain largely unclear. Of particular interest is that intra-amyloid lipids have been detected in the kidney of the previously reported Glu34Lys AApoAI patient.[16] Also intriguing is the finding, here, that apoA-I fibrils are deposited at the choriodal capillaris/retinal pigment epithelium (RPE)/Bruch's membrane (BrM) complex, a highly specialized structure acting, like the glomerular membrane, as a molecular sieve regulating the filtration of HDLs which play a major role for intra-retinal lipid transport.[34,35] The choroid_RPE_BrM complex is also the site of accumulation of liproteins/lipids before deposition of drusen amyloid-like vesicles in patients affected by age-related macular degeneration.[36] Drusen amyloid-like vesicles represent a complex macromolecule assembly in which wild-type apoA-I, along with apoE, SAP, clusterin and complement proteins, are co-deposited with the Aß peptide.[36] Another unexplained feature in AApoAI is the fact that AApoAI patients do not show an increased risk of premature cardiovascular diseases (CVD), despite their lower efficiency at forming HDL particles. It has recently been proposed that some amyloidogenic apoA-I variants have a higher efficiency at catalysing cholesterol efflux from macrophages, suggesting that specific HDL subpopulation might be associated with AApoAI.[37] This paradox is also a characteristic of very rare particular non-amyloidogenic apoA-I variants, such as Milano (Arg173Cys) and Paris (Arg151Cys) mutant forms of apoA-I, which form non-native disulphide bonds between the apoA-I variants and other cysteine-containing apolipoproteins present on HDLs, namely apoA-II and apo-E.[38] These "cardioprotective" apoA-I mutants are associated with reduced HDL plasma levels and reduced particle size, resulting from the dimerization of apoA-I induced by the

presence of a cysteine residue in the mutant protein.[38] Similarly to AFib amyloidosis,[39] no mutations creating a cysteine residue have been associated with AApoAI, except the two frameshift variants reported here, p.His179Profs*47 and p.Thr185Alafs*41 (p.His155Profs : APMWTRCARIWPPTATSCASAWPRALRLSRRTAAPDWPSTTPRPPSI and p.Thr185Alafs : RPRIWPPTATSCASAWPRALRLSRRTAAPDWPSTTPRPPSI). These frameshift variants are expected to contain a premature stop codon at amino acid position 201, leading to a shorter apoA-I proteins whose last C-terminal residues contain non-native cysteines. A first attempt had shown that p.His179Profs*47 might form a disulfide bridge with itself and apoA-II, but absence of available additional plasma samples do not allow us, as yet, to confirm this preliminary data that needs to be fully explored in a larger patient population. Although much remains to be investigated, the p.His179Profs*47 and p.Thr185Alafs*41 variants are unusual variants coding for truncated cysteine-containing apoA-I proteins that are amyloidogenic *in vivo*, providing a unique opportunity to better understand the mechanisms by which apoA-I participates in reverse cholesterol transport as well as the mechanisms which render specific apoA-I variants amyloidogenic

In summary, we report as-yet unrecognized clinical forms of AApoAI revealing that the retina is a new target tissue for apoA-I fibril deposition, offering a unique challenging monogenic amyloid retinal model. This study emphasizes the remarkable symptomatic benefits of combined hepatorenal transplantation that must encourage interdisciplinary collaboration between Nephrologists and Ophthalmologists to ensure appropriate management of AApoAI patients. Finally, we provide compelling evidence that AApoAI may present with distinct amyloid distribution inside the kidney, yielding an uncommon example for the same amyloid precursor protein.

METHODS

Genetics

Blood samples from all individuals were obtained after their written informed consent. This study had the approval of the Ethics Committee of the Hospital of Poitiers, Limoges and Rennes and was performed according to the Declaration of Helsinki. Genomic DNAs were extracted from whole blood treated with EDTA using the PreAnalytiX kit (Qiagen, Valencia, CA) and all coding exons and flanking intronic sequences of *APOA1* were amplified by polymerase chain reaction amplification (PCR) as previously described.[40] The resulting PCR products were purified using the QIA quick PCR purification kit (Qiagen, Valencia, CA), and sequenced on both strands using dye terminator chemistry (BigDye Terminator cycle Sequencer, Applied Biosystem, Foster City, CA) combined with an ABI 3730 DNA automated sequencer (Applied Biosystem, Frankfurt, Germany). DNA numbering of mutation was based on the *APOA1* cDNA sequence (GenBank accession number NM_000483.4). For cDNA numbering, position +1 corresponds to the A of the ATG-translation initiation codon of the apoAI protein in the reference sequence (RefSeq NM_000039).

Light microscopy, immunofluorescence and immunohistochemistry

Biopsy samples were processed for light microscopic and immunofluorecsence studies, as previously described.[40] Paraffin-embedded tissue samples were examined after conventional (hematoxylin-eosin, periodic-acid Schiff) and special staining including Masson's trichrome, toluidine blue, and Marinozzi's silver staining, using standard methods. 6-mm-thick sections from formalin fixed paraffin-embedded renal biopsies were stained for amyloid with Congo red and viewed under crossed polarized light. Immunofluorescence and immunohistochemistry studies were performed on 5µm cryosections using an anti-apoA-I monoclonal antibody (Dako, Carpenteria, CA), and other monospecific antibodies against serum amyloid A protein, lysozyme, fibrinogen, transthyretin, and kappa and lambda immunoglobulin light chains, as previously described.[33] Specificity of staining was confirmed by prior absorption of the antiserum with pure antigen in each case, and positive and negative controls were included.

Transmission electron microscopy

Kidney samples were processed for transmission electron microscopy as previously described.[40] Briefly, kidney samples were fixed with 4% glutaraldehyde in phosphate buffer (0.1 M; pH = 7, 4) for one hour at 4°C. Samples were then washed three times (3x10 min) in phosphate-buffered saline (PBS) at pH 7,4 before being post-fixed in osmium tetroxyde 1% in phosphate buffer 0,1M for one hour at 4°C, processed through a graded acetone series, embedded in araldite (Fluka, Buchs, Switzerland) and polymerised overnight at 60°C. Thin sections (60 nm) were cut with a diamond knife on Reichert Ultracut S, recovered on Cu grids, contrasted with uranyl acetate (4%) and lead citrate and observed under a JEOL 1010 transmission electron microscope (Jeol Ltd, Tokyo, Japan). To confirm the fibrillar nature of the deposits, appropriate areas were examined at X50,000.

Immunogold labeling

Immunogold labeling was performed as previously described, and thin sections (80nm) were cut from glutaraldehyde-fixed and collected on nickel grids.[40] Grids were floated

on one drop of 5% sodium metaperiodate (Sigma Chemical Co, St Louis) in PBS for 30 min. Sections were washed with PBS three times and then saturated for one hour with 3% BSA in PBS in order to minimize non-specific labelling. Grids were then incubated overnight at 4°C with a 1/20 dilution of monoclonal mouse anti-human apoA1 antibody (AbCys S.A). Sections were washed six times in PBS-BSA 0,3%, and incubated for one hour with a 1/20 dilution of anti-mouse IgG gold conjugate (Sigma Chemical Co, USA). Specificity of the immunostaining procedure was established by omission of the primary antibody and incubation with the immunogold conjugate only. Immunolabelled sections were contrasted using uranyl acetate and observed under a JEOL 1010 transmission electron microscope (Jeol Ltd, Tokyo, Japan).

MS-based proteomic typing of amyloid deposits

We used a previously established proteomics method for typing the amyloid deposits.[41] Ten-micrometer-thick sections of formalin-fixed paraffin-embedded tissue were mounted on slides (Expression Pathology) and stained with hematoxylin and eosin. One hundred thousand square micro- meters of deposits were selected by laser microdissection (Leica 6500; Leica Microsystems). Proteins were extracted from the collected material in ammonium bicarbonate buffer, reduced with dithiothreitol, and alkylated with iodoacetamide. Then, proteins were digested into peptides with trypsin (Sigma) and analyzed by nanoscale liquid chromatography (LC), coupled with tandem MS (MS/MS), using an UltiMate 3000 RSLCnano System (Dionex) coupled to an Linear Trap Quadripole Orbitrap Velos mass spectrometer (Thermo Fischer Scientific). MS data files were analyzed using Mascot (version 2.5.2) to search either the SwissProt or the National Center for Biotechnology Information database. All positive samples were further examined using an expanded Swissprot database containing all the previously reported *APOA1* variants.Validation of results was performed through a false- discovery rate set to 1% at protein and peptide-sequence match levels determined by target-decoy search using the in-house–developed Proline software (http://proline.profiproteomics.fr/). The spectral count metrics was used to rank the proteins and peptides according to their relative abundance in the sample.

DISCLOSURE

All the authors declared no competing interests.

ACKNOWLEDGEMENTS

We thank family members of the patients for their participation in this study. This work was supported by the Association Française Contre l'Amylose. We thank Ahmet Dogan for help at early stages of proteomics analysis. We thank Mathilde Camus and Brigitte Nedelec for their assistance with proteomics analyses and figure preparation, respectively. We also thank Dr Hélène Toure-Manic for her ophthalmological investigations on patient III.3 of family C.

AUTHOR CONTRIBUTIONS

MC performed part of anatomopathological studies and proteomics analysis of all affected tissues by LC-MS/MS, and downstream data interpretation. JCA, VJ, ED, TF, AT, JPR and FB recruited patients and gathered detailed renal clinical information. CB performed mutation analysis. PRR, AB, and performed ophtalmological investigations including ICG angiography and downstream data analysis. AD, and DS performed combined hepatorenal tranplantation. JMG, NRL, NQ, FP performed anatomopathological analysis including Congo red staining, immunohistochemical studies, electron and immunoelectron microscopy analysis. SV conceived, directed, supervised all data of the study, performed genotype–phenotype correlation, and wrote the manuscript. All authors approved the final version. The corresponding author (SV) had full access to all the data in the study and had final responsibility for the decision to submit for publication.

1. Rosenson RS, Brewer HB, Jr., Davidson WS, et al. Cholesterol efflux and atheroprotection: advancing the concept of reverse cholesterol transport. *Circulation*. 2012;125(15):1905-19.

2. Sorci-Thomas, MG. & Thomas, MJ. The effects of altered apolipoprotein A-I structure on plasma HDL concentration. *Trends Cardiovasc. Med.* 2002;12:121–128.

3. Nichols WC, Dwulet FE, Liepnieks J, et al. Variant apolipoprotein AI as a major constituent of a human hereditary amyloid. *Biochem Biophys Res Commun*. 1988;156(2):762-8.

4. Obici L, Bellotti V, Mangione P, et al. The new apolipoprotein A-I variant leu(174) --> Ser causes hereditary cardiac amyloidosis, and the amyloid fibrils are constituted by the 93-residue N-terminal polypeptide. *Am J Pathol.* 1999;155(3):695-702.

5. Gursky O, Mei X, and Atkinson D. The crystal structure of the C-terminal truncated apolipoprotein A-I sheds new light on amyloid formation by the N-terminal fragment. *Biochemistry.* 2012;51(1):10-8.

6. Das M, Wilson CJ, Mei X, et al. Structural stability and local dynamics in disease-causing mutants of human Apolipoprotein A-I: what makes the protein amyloidogenic? *Journal of molecular biology.* 2016;428:449-62.

7. Morgado I, Panahi A, Burwash AG, et al. Molecular insights into human hereditary : Apolipoprotein A‑I amyloidosis caused by the Glu34Lys mutation. *Biochemistry.* 2018; 57:5738-5747.

8. Rowczenio DM, Noor I, Gillmore JD, et al. Online registry for mutations in hereditary amyloidosis including nomenclature recommendations. *Hum Mutat.* 2014;35(9):E2403-12.

9. Nichols WC, Gregg RE, Brewer HB Jr,et al. A mutation in apolipoprotein A-I in the Iowa type of familial amyloidotic polyneuropathy. *Genomics.* 1990;8:318–323.

10. Rowczenio D, Dogan A, Theis JD, et al. Amyloidogenicity and clinical phenotype associated with five novel mutations in apolipoprotein A-I. *Am J Pathol.* 2011;179(4):1978-87.

11. Lachmann HJ, Booth DR, Booth SE et al. Misdiagnosis of hereditary amyloidosis as AL (primary) amyloidosis. *N. Engl. J. Med.* 2002; 346:1786–91.

12. Gregorini G, Izzi C, Obici L, et al. Renal apolipoprotein A-I amyloidosis: a rare and usually ignored cause of hereditary tubulointerstitial nephritis. *J Am Soc Nephrol.* 2005;16(12):3680-6.

13. Gregorini G, Izzi C, Ravani P, et al. Tubulointerstitial nephritis is a dominant feature of hereditary apolipoprotein A-I amyloidosis. *Kidney Int.* 2015;87(6):1223-9.

14. Traynor CA, Tighe D, O'Brien FJ, et al. Clinical and pathologic characteristics of hereditary apolipoprotein A-I amyloidosis in Ireland. *Nephrology.* 2013;18:549–54.

15. Eriksson M, Schonland S, Yumlu S, et al. Hereditary apolipoprotein AI-associated amyloidosis in surgical pathology specimens: Identification of three novel mutations in the APOA1 gene. *J Mol Diagn.* 2009;11:257–62.

16. Andeen NK, Lam DY, de Boer IH, and Nicosia RF. Renal ApoA-1 amyloidosis with Glu34Lys mutation and intra-amyloid lipid accumulation. *J Am Soc Nephrol*. 2014;25(12):2703-5.

17. Dogan A. Amyloidosis : insigths from proteomics. *Annu Rev Pathol.* 2017;12:277-304.

18. Benson MD, Liepnieks J, Uemichi T,et al. Hereditary renal amyloidosis associated with a mutant fibrinogen alpha-chain. *Nat Genet.* 1993;3:252–255.

19. Benson MD, Liepnieks JJ, Yazaki M, et al. A new human hereditary am- yloidosis: The result of a stop-codon mutation in the apolipoprotein AII gene. *Genomics.* 2001;72:272–277.

20. Pepys MB, Hawkins PN, Booth DR, et al. Human lysozyme gene mutations cause hereditary systemic amyloidosis. *Nature.*1993;362: 553–557.

21. Levy E, Haltia M, Fernandez-Madrid I, Koivunen O, Ghiso J, Prelli F, Frangione B: Mutation in gelsolin gene in Finnish hereditary amyloidosis. *J Exp Med.* 1990;172:1865–1867.

22. Efebera YA, Sturm A, Baack EC, et al. Novel gelsolin variant as the cause of nephrotic syndrome and renal amyloidosis in a large kindred. *Amyloid.* 2014;21(2):110-2.

23. Valleix S, Verona G, Jourde-Chiche N, et al. D25V apolipoprotein C-III variant causes dominant hereditary systemic amyloidosis and confers cardiovascular protective lipoprotein profile. *Nat Commun.* 2016;7:10353.

24. Nasr SH, Dasari S, Hasadsri L, et al. Novel type of renal amyloidosis derived from apolipoprotein-CII. *J Am Soc Nephrol.* 2017;28(2):439-445.

25. Beirão JM, Malheiro J, Lemos C, et al. Ophthalmological manifestations in hereditary transthyretin (ATTR V30M) carriers: a review of 513 cases. *Amyloid.* 2015; 22(2):117–122.

26. Reynolds MM, Veverka KK, Gertz MA, et al. Ocular manifestations of familial transthyretin amyloidosis. *Am J Ophthalmol.* 2017;183:156-162.

27. Rousseau A, Terrada C, Touhami S, et al. Angiographic signatures of the predominant form of transthyretin amyloidosis (Val30Met mutation). *Am J Ophthalmol.* 2018;192:169-177.

28. Gillmore JD, Stangou AJ, Tennent GA, et al. Clinical and biochemical outcome of hepatorenal transplantation for hereditary systemic amyloidosis associated with apolipoprotein Gly26Arg. *Transplantation.* 2001;71(7):986-92.

29. Gillmore JD, Stangou AJ, Lachmann HJ, et al. Organ transplantation in hereditary apolipoprotein AI amyloidosis. *Am J Transplant.* 2006;6(10):2342-7.

30. Scalvini T, Martini PR, Gambera A, et al. Spermatogenic and steroidogenic impairment of the testicle characterizes the hereditary leucine-75-proline apolipoprotein a-I amyloidosis. *J Clin Endocrinol Metab*. 2008;93(5):1850-3.

31. Haase CL, Frikke-Schmidt R, Nordestgaard BG, et al. Population-based resequencing of APOA1 in 10,330 individuals: spectrum of genetic variation, phenotype, and comparison with extreme phenotype approach. *PLoS Genet.* 2012;8(11):e1003063.

32. Gillmore JD, Booth DR, Rela M, et al. Curative hepatorenal transplantation in systemic amyloidosis caused by the Glu526Val fibrinogen alpha-chain variant in an English family. *QJM.* 2000;93(5):269-75.

33. Marchesi M, Parolini C, Valetti C, et al. The intracellular quality control system down-regulates the secretion of amyloidogenic apolipoprotein A-I variants: a possible impact on the natural history of the disease. *Biochim Biophys Acta.* 2011;1812(1):87-93.

34. Fliesler SJ, Bretillon L. The ins and outs of cholesterol in the vertebrate retina. *J Lipid Res.* 2010;51(12):399-413.

35. Curcio CA, Johnson M, Rudolf M, et al. The oil spill in ageing Bruch membrane. *Br Ophthalmol.* 2011;95(12):1638-1645.

36. Li CM, Clark ME, Chimento MF, et al. Apolipoprotein localizatio in isolated drusen and retinal apolipoprotein gene expression. Invest Ophthalmol Vis Sci. 2006;47(7):3119-3128.

37. Del Giudice R, Domingo-Espin J, Iacobucci, et al. Structural determinants in ApoA-I amyloidogenic variants explain improved cholesterol metabolism despite low HDL levels. *Biochim Biophys Acta Mol Basis Dis.* 2017;1863(12):3038-3048.

38. Weisgraber KH, Bersot TP, Mahley RW, et al. A-I milano apoprotein. Isolation and characterization of a cysteine-containing variant of the A-I protein from human high density lipoproteins. J Clin Invest. 1980;66(5):901-907.

39. Garnier C, Briki F, Nedelec B, et al. VLITL is a major cross-β-sheet signal for fibrinogen A α-chain frameshift variants. *Blood.* 2017; 130(25): 2799-2807.

40. Valleix S, Gillmore JD, Bridoux F, et al. Hereditary systemic amyloidosis due to Asp76Asn ß2-microglobulin. *N Engl J Med.* 2012;366(24):2276-83.

41. Sethi S, Vrana JA, Theis JD, et al. Laser microdissection and mass spectrometry-based proteomics aids the diagnosis and typing of renal amyloidosis. *Kidney Int.* 2012;82:226–234.

FIGURE LEGENDS

Figure 1 AApoA-I associated with Glu34Lys variant. (**a and b**) Pedigrees and segregation of Glu34Lys in families A and B. +/- designates the heterozygous Glu34Lys mutation; -/- designates absence of Glu34Lys. Blue arrows indicate the generation in which *APOA1* mutation has occurred *de novo*. (**c**) Abdominal CT scan showing calcified adrenal glands (yellow arrows) (**d**) Sequence chromatograph of the heterozygous c.172G>A;Glu34Lys mutation in exon 3 of *APOA1*.

Figure 2 AApoA-I associated with p.His179Profs*47 variant**.** (**a-c**) Pedigrees and segregation of p.His179Profs*47 in families C, D, and E. +/- designates the heterozygous p.His179Profs*47 mutation; -/- designates absence of p.His179Profs*47 on both alleles. Blue arrows indicate the generation in which *APOA1* mutation has occurred *de novo* (**d**) Sequence chromatograph of the heterozygous p.His179Profs*47 mutation in exon 4 of *APOA1*.

Figure 3 AApoA-I associated with p.Thr185Alafs*41 variant. (a) The pedigree and segregation of p.Thr185Alafs*41 in family F. +/- designates the heterozygous p.Thr185Alafs*41 mutation; -/- designates absence of p.Thr185Alafs*41 on both alleles. Blue arrows indicate the generation in which *APOA1* mutation has occurred *de novo* (**b**) Sequence chromatograph of the heterozygous p.Thr185Alafs*41 mutation in exon 4 of *APOA1*.

Figure 4 Ophthalmologic features of AApoAI patients with Glu34Lys and frameshift variants from proband III.3 of family A. (**a**) Color fundus photograph of both eyes from proband III.3 of family A shows yellowish lesions around and irradiating from the optic disc. (**b**) ICGA shows diffuse hyperfluorescent spots and linear hyperfluorescent lesions along the large choroidal vessels at the posterior pole from proband III.3 of family A. (**c**) Similar abnormal ICGA choroidal lesions were observed from proband II.1 of family D.

Figure 5 Anatomopathological renal characteristics associated with AApoAI p.His179Profs*47 and p.Thr185Alafs*41 variants. (a) (b) Congo Red staining of kidney specimen derived from patient III.3 of family C revealing reddish-orange amyloid deposits (yellow arrows) with corresponding apple-green birefringence under polarized light in glomeruli (Original magnifications 200X). **(c)** Silver-stained renal biopsy showing amyloid deposits closely associated with focal disappearance and duplication of the glomerular basement membranes (Original magnification 400X). **(d)** Electron micrograph showing randomly unbranched fibrils with a diameter of approximately 10 nm in the glomerular compartment, mainly in the sub-epithelial space (Original magnification 80000X). **(e)** Electron micrograph highlighting amyloid fibrils in glomeruli (Original magnification 3000X). **(f)** High magnification of electron micrograph showing extramembranous fibrillar deposits (Original magnification 15000X). **(g)** Electron micrograph demonstrating no amyloid fibril material in the interstitial compartment (Original magnification 6000X). **(h)** Immunofluorescence showing strong

immunoreactivity of glomerular amyloid deposits for anti-apoAI antibody (Original magnification 400X). (**i**) Electron micrograph showing immunogold labeling with anti-apoAI antibody of glomerular amyloid fibrils (Original magnification 40000X).

Figure 6 Anatomopathological characteristics of affected tissues associated with AApoAI Glu34Lys variant. (a) (b) Congo Red staining of kidney (patient III.3, family A), revealing reddish-orange amyloid deposits (yellow arrows) with corresponding apple-green birefringence under polarized light (Original magnifications 200X). **(c) (d)** Jones silver staining of kidney from patient II.3 of family A shows glomerular expansion by an amorphous, pale, « cotton candy » material that corresponds to amyloid deposits within the mesangium (yellow star) and the capillary loops. The capillary loops are thickened due to subendothelial deposition and subepithelial deposition associated with spike reaction (yellow arrow) (Original magnifications 100X). **(e) (f)** Congo Red staining of liver (patient II.4, family B), and heart (patient II.3, family A) revealing reddish-orange amyloid deposits (yellow arrows) with corresponding apple-green birefringence under polarized light. (Original magnifications 200X).

Figure 7 Anatomopathological characteristics of affected tissues associated with AApoAI Glu34Lys variant. (a) (b) Congo Red staining of testis specimen derived from patient II.4 of family B revealing reddish-orange amyloid deposits with corresponding apple-green birefringence under polarized light (yellow arrows) (Original magnifications 200X). **(c) (d) (e) (f)** Congo Red staining of retina derived from patient II.4 of family B revealing reddish-orange amyloid deposits with corresponding apple-green birefringence under polarized light (yellow arrows) at different magnifications (Original magnifications 200X and 400X).

Figure 8 Mass spectrometric analyses of AApoAI Glu34Lys variant. (**a, b)** Renal and liver amyloid proteome, respectively, indicating the presence of apoA-I in fibrils, along with the "amyloid signature" proteins, apoE and SAP.

Figure 9 Mass spectrometric analyses of AApoAI Glu34Lys variant. (**a, b)** Heart and testicular amyloid proteome, respectively, indicating the presence of apoA-I in fibrils, along with the "amyloid signature" proteins, apoE and SAP.

Figure 10 Mass spectrometric analyses of AApoAI Glu34Lys variant. (a) Retinal amyloid proteome with the presence of apoA-I in fibrils, along with the "amyloid signature" proteins, apoE and SAP. (**b**) ApoA-I tryptic digestion followed by MS identified the mutation-containing peptide fragment (in blue) with lysine at position 58 of pre-apoA-I in red (nomenclature includes amino acids coding for the signal peptide, which corresponds to Lys34 of the mature protein).

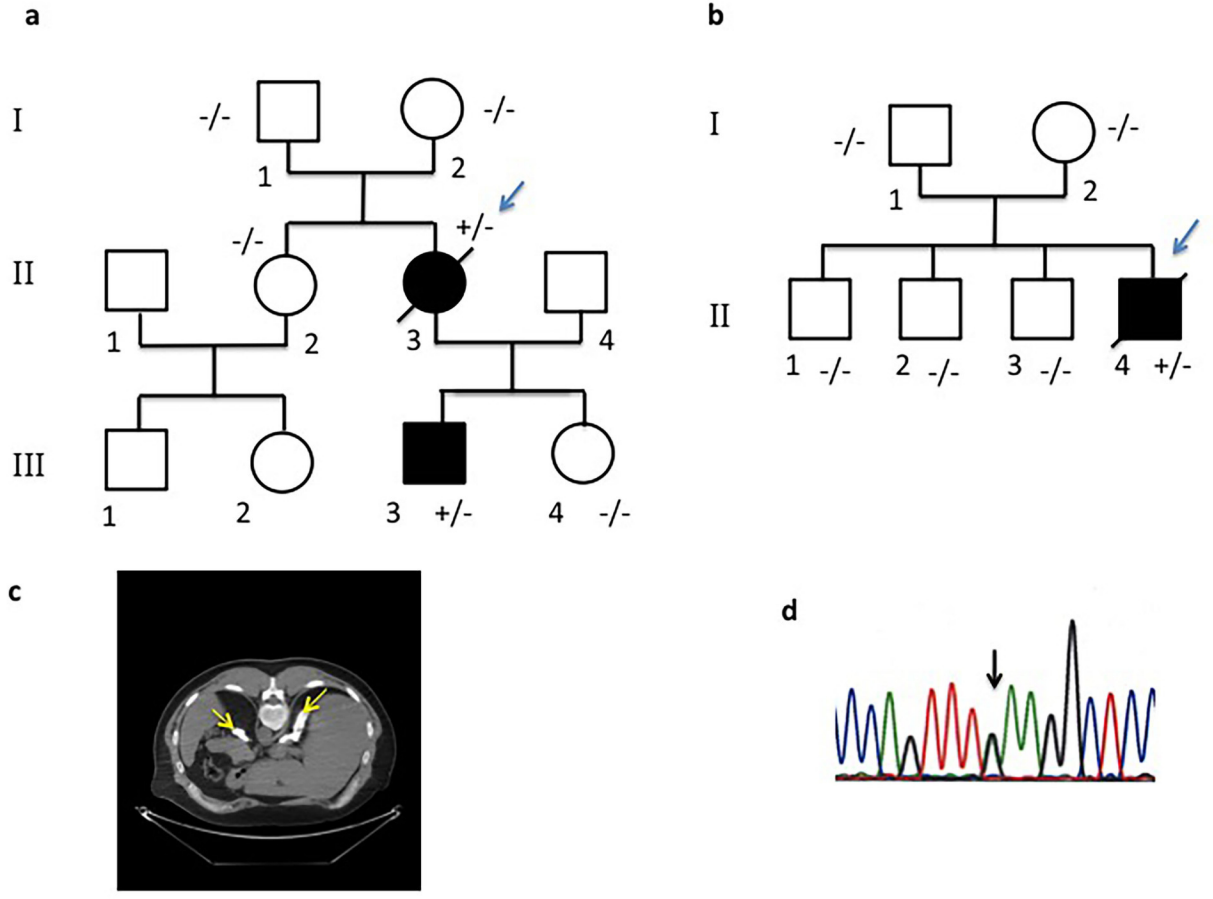
a
I
II
III
-/-
-/-
1
2
-/-
+/-
1
2
3
4
1
2
3 +/-
4 -/-
b
I
II
-/-
-/-
1
2
1 -/-
2 -/-
3 -/-
4 +/-
c
d

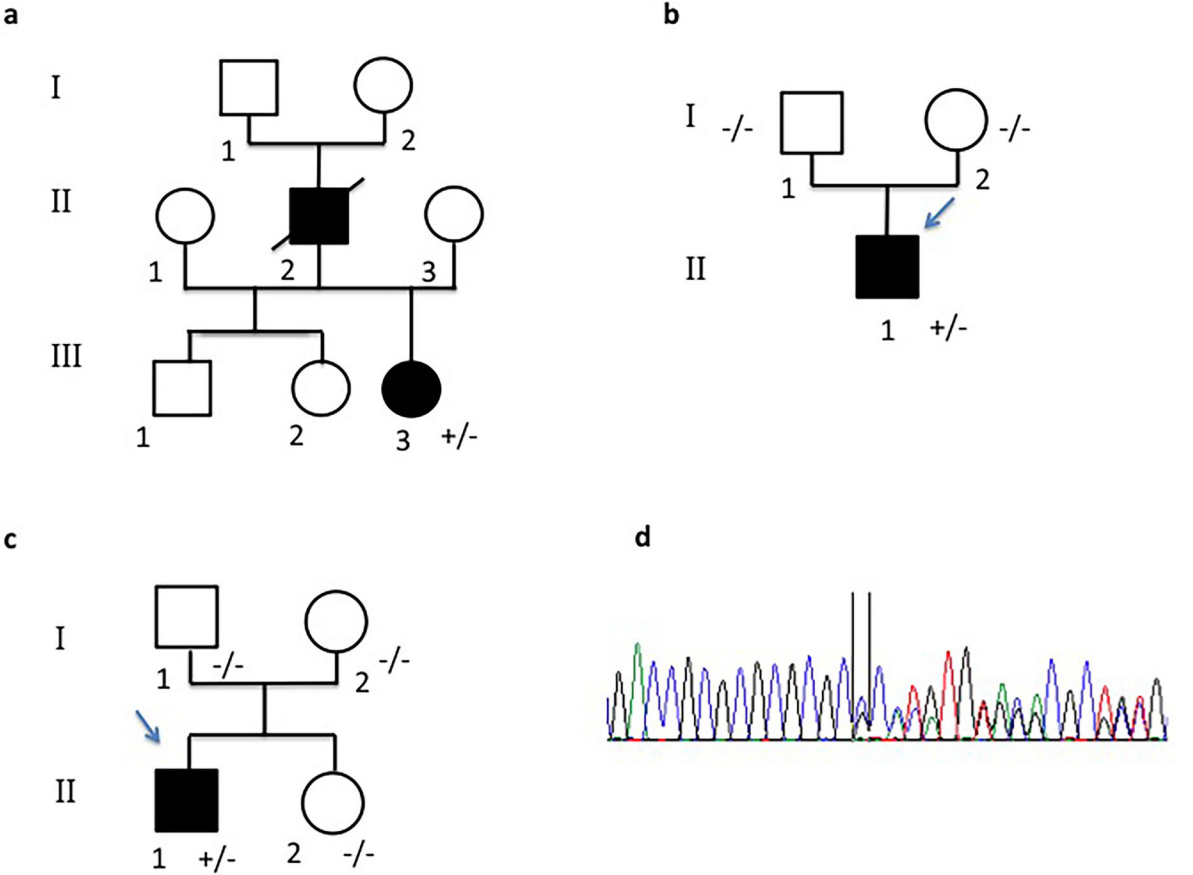
a
I
1
2
II
1
2
3
III
1
2
3 +/-
b
I -/-
-/-
1
2
II
1 +/-
c
I
1 -/-
2 -/-
II
1 +/-
2 -/-
d

a

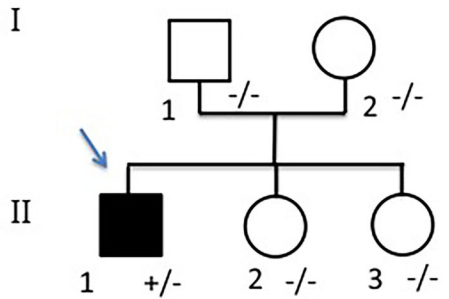

b

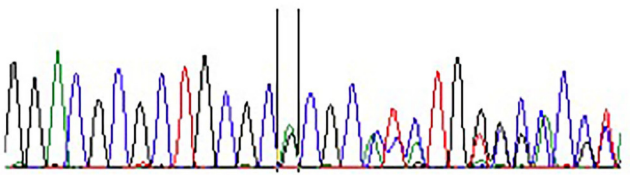

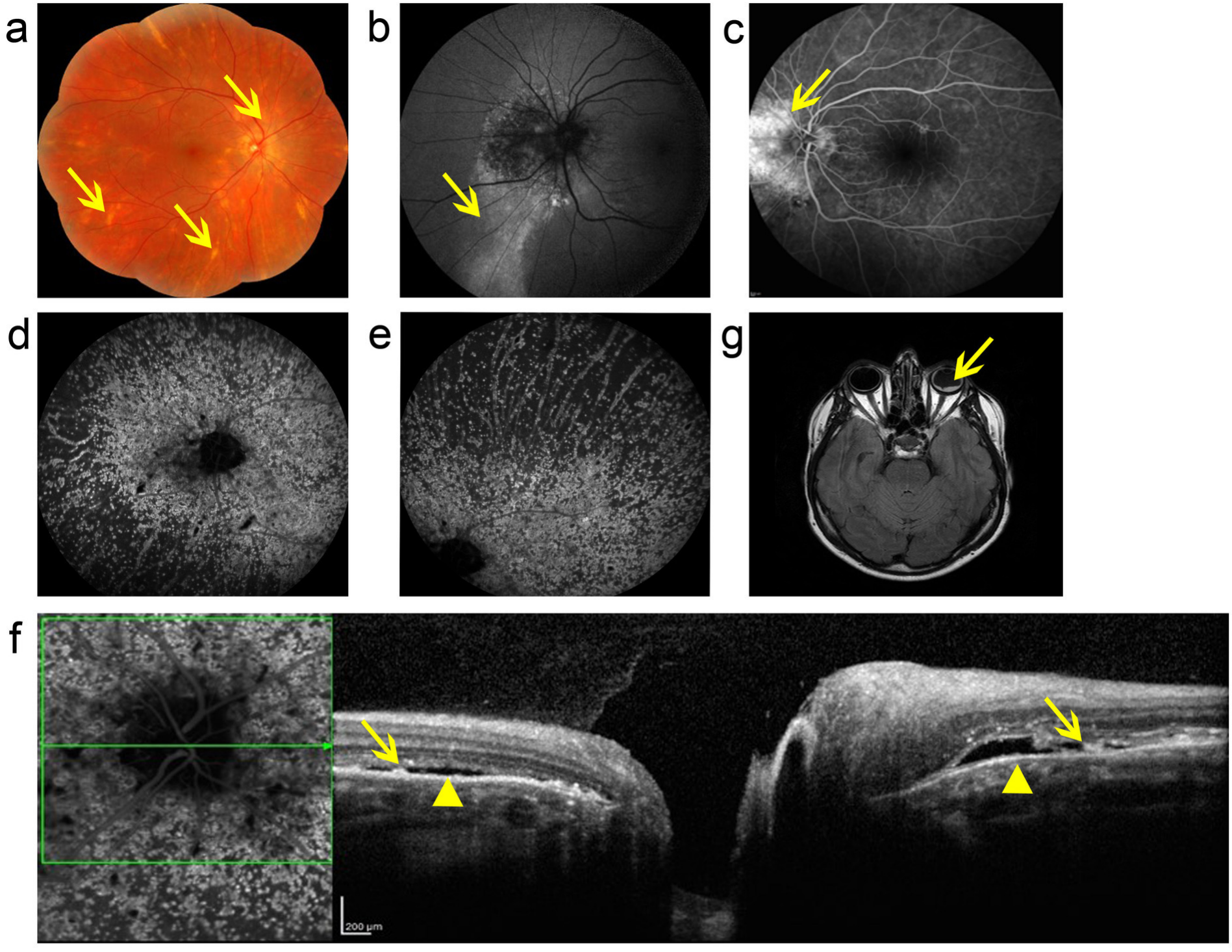
a
b
c
d
e
g
f
200 µm

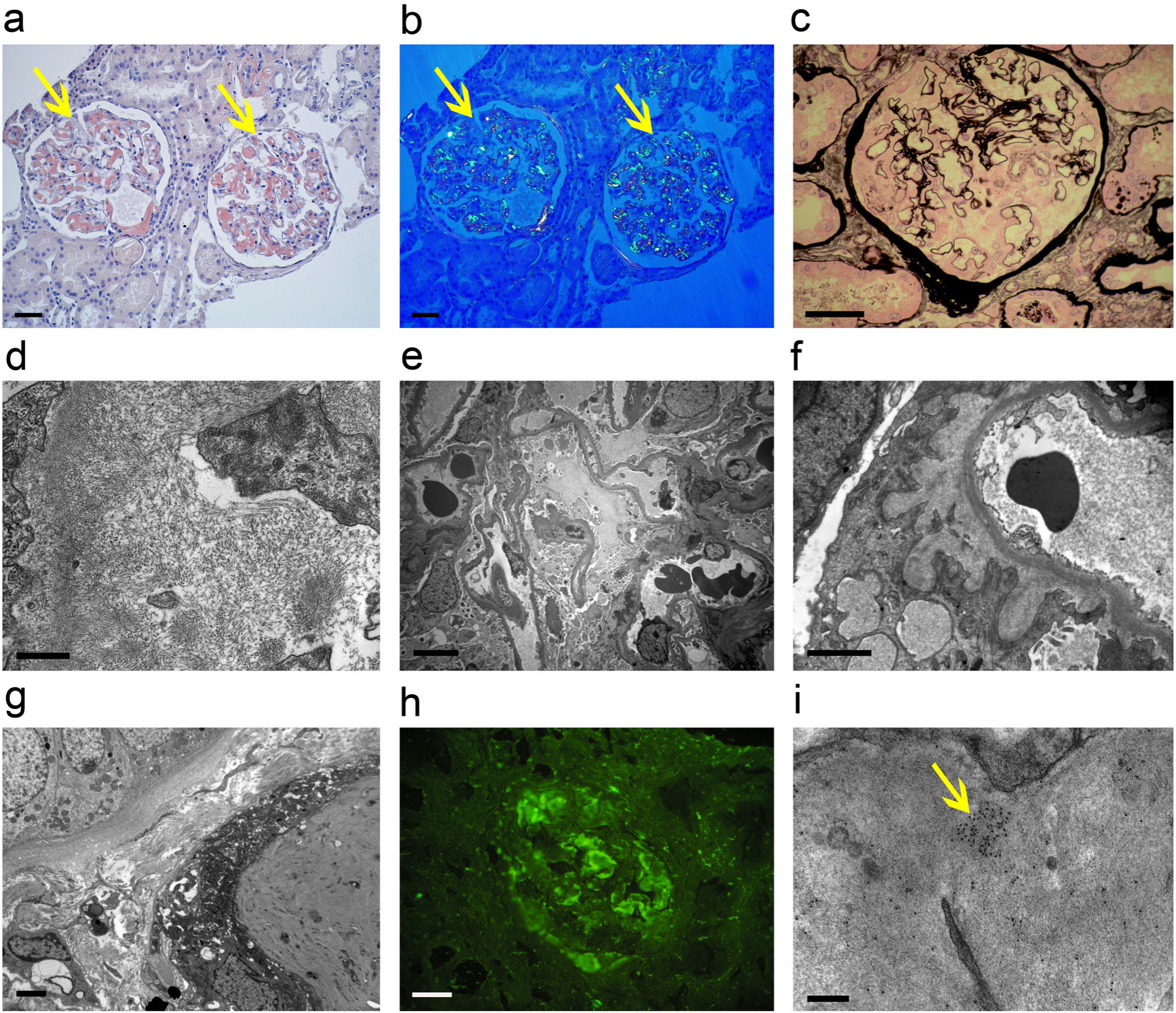
a
b
c
d
e
f
g
h
i

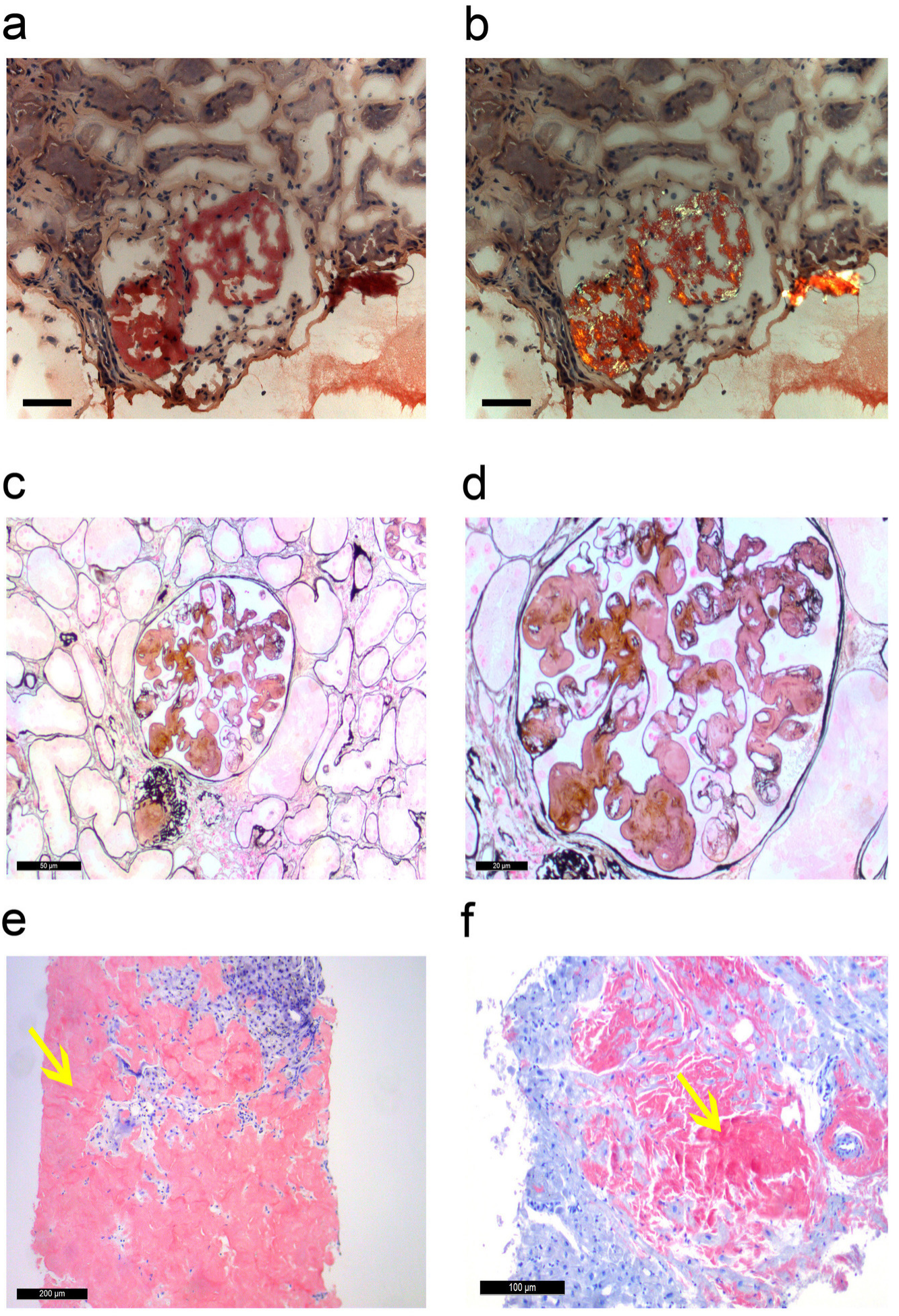
a
b
c
50 µm
d
20 µm
e
200 µm
f
100 µm

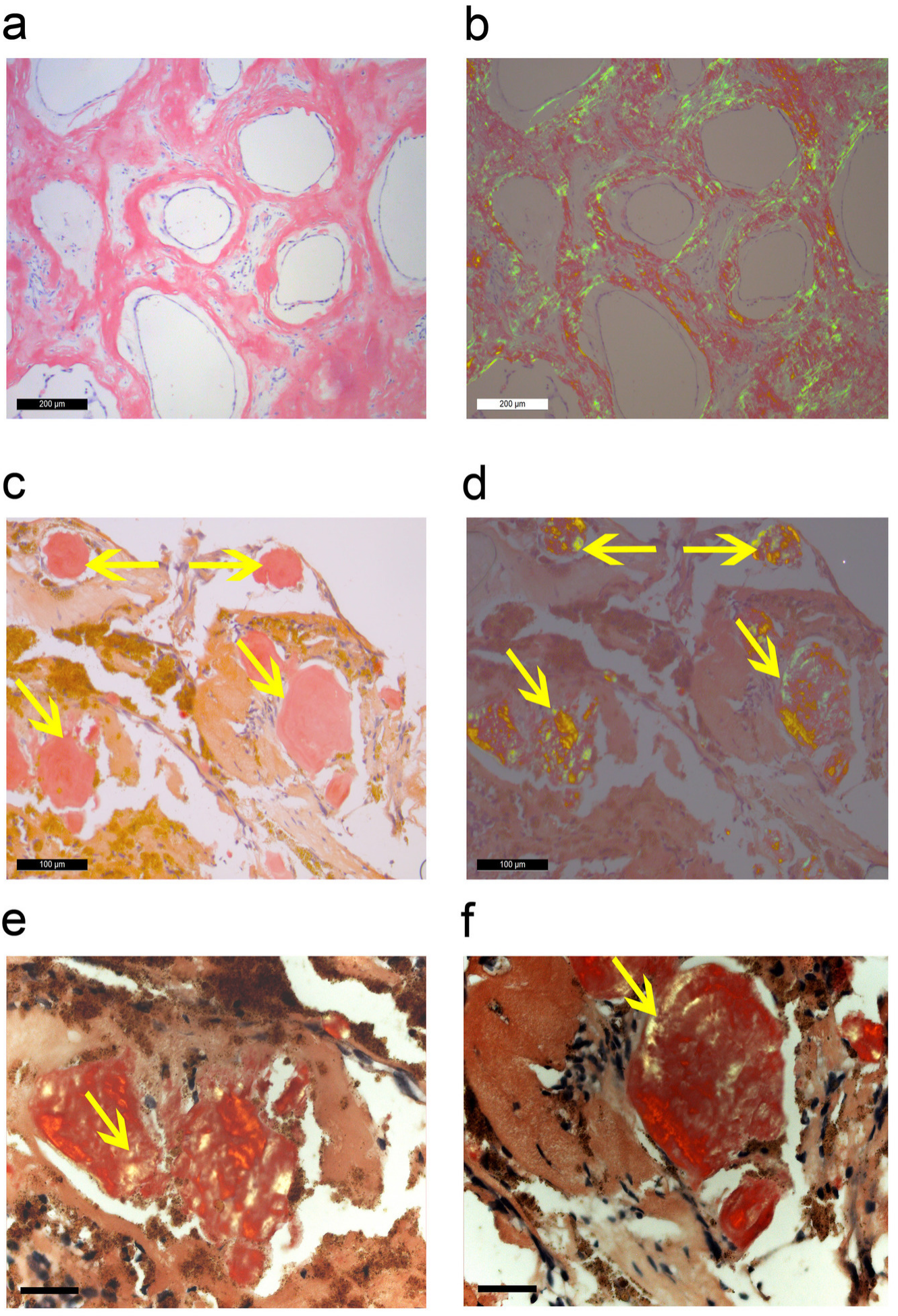
a
200 µm
b
200 µm
c
100 µm
d
100 µm
e
f

a

Identified proteins	Accession number	MW(kDa)	Sample
Apolipoprotein A-I	APOA1	31	25
Collagen alpha-3(VI) chain	COL6A3	110	20
Serum albumin	ALB	71	19
Complement C3	C3	189	18
Vitronectin	VTN	55	15
Apolipoprotein E	APOE	36	14
Serotransferrin	TF	190	14
Clusterin	CLU	53	13
Complement factor H-related protein 1	CFHR1	144	11
Complement component C9	C9	16	10
Serum amyloid P-component	APCS	25	9
Vimentin	VIM	54	9
Complement C4-A	C4A	194	7
Actin, cytoplasmic 1	ACTB	42	7
Fibulin-1	FBLN1	81	7
Complement C4-B	C4B	194	6
Complement factor H	CFH	65	5
Actin, alpha cardiac muscle 1	ACTC1	42	4

b

Identified proteins	Accession number	MW(kDa)	Sample
Vitronectin	VTNC_HUMAN	55	52
Serum amyloid P-component	SAMP_HUMAN	25	48
Apolipoprotein A-I	APOA1_HUMAN	31	44
Apolipoprotein E	APOE_HUMAN	36	44
Complement C3	CO3_HUMAN	189	35
Hemoglobin subunit beta	HBB_HUMAN	15	29
Collagen alpha-1(VI) chain	CO6A1_HUMAN	110	24
Fibrillin-1	FBN1_HUMAN	333	22
Serum albumin	ALBU_HUMAN	71	22
Actin, cytoplasmic 1	ACTB_HUMAN	42	19
Hemoglobin subunit delta OS	HBD_HUMAN	16	18
Complement component C9	HBD_HUMAN	16	18
Complement factor H	CO9_HUMAN	65	18
Complement factor H-related protein 1	CFAH_HUMAN	144	16
Vimentin	VIME_HUMAN	54	15
Hemoglobin subunit alpha	HBD_HUMAN	162	14
Complement C4-B	CO4B_HUMAN	194	14
Basement membrane-specific heparan sulfate proteoglycan core protein	PGBM_HUMAN	479	14

a

Identified proteins	Accession number	MW(kDa)	Sample
Vitronectin	VTNC_HUMAN	55	121
Serum albumin	ALBU_HUMAN	71	57
Collagen alpha-3(VI) chain	CO6A3_HUMAN	345	54
Basement membrane-specific heparan sulfate proteoglycan core protein	PGBM_HUMAN	479	53
Apolipoprotein E	APOE_HUMAN	36	47
Serum amyloid P-component	SAMP_HUMAN	25	45
Filamin-A	FLNA_HUMAN	283	44
Actin, cytoplasmic 1	ACTB_HUMAN	42	39
Actin, aortic smooth muscle	ACTA_HUMAN	42	34
Fibrillin-1	FBN1_HUMAN	333	33
Complement component C9	CO9_HUMAN	65	31
Apolipoprotein A-I	APOA1_HUMAN	31	31
Lactotransferrin	TRFL_HUMAN	80	25
Laminin subunit beta-2	LAMB2_HUMAN	203	21
Clusterin	CLUS_HUMAN	53	17
Desmin	DESM_HUMAN	54	17
Collagen alpha-1(VI) chain	CO6A1_HUMAN	110	16
Hemoglobin subunit beta	HBB_HUMAN	15	16

b

Identified proteins	Accession number	MW(kDa)	Sample
Serum albumin	ALBU_HUMAN	71	73
Myosin	MYH7_HUMAN	224	73
Apolipoprotein A-I	APOA1_HUMAN	31	41
Apolipoprotein E	APOE_HUMAN	36	35
Keratin, type II cytoskeletal 6	K2C6_HUMAN	60	35
Vitronectin	VTNC_HUMAN	55	33
Vimentin	VIME_HUMAN	54	21
Serum amyloid P-component	SAMP_HUMAN	25	20
Actin, alpha cardiac muscle	ACTC_HUMAN	42	20
Apolipoprotein A-IV	APOA4_HUMAN	45	17
Actin, cytoplasmic	ACTB_HUMAN	42	16
Clusterin	CLUS_HUMAN	53	15
Hemoglobin subunit alpha	HBA_HUMAN	15	10
Myosin light chain	MYL3_HUMAN	22	10
Hemoglobin subunit beta	HBB_HUMAN	16	8
Myoglobin	MYG_HUMAN	17	7
Immunoglobulin kappa constant	IGKC_HUMAN	12	5
Fatty acid-binding protein	FABPH_HUMAN	15	3

a

Identified proteins	Accession number	MW(kDa)	Sample
Apolipoprotein A-I	APOA1_HUMAN	31	44
Vitronectin	VTNC_HUMAN	55	14
Apolipoprotein E	APOE_HUMAN	36	12
Serum albumin	ALBU_HUMAN	71	9
Clusterin	CLUS_HUMAN	53	9
Keratin, type II cytoskeletal 1	K2C1_HUMAN	66	8
Histidine-rich glycoprotein	HRG_HUMAN	60	6
Keratin, type I cytoskeletal 9	K1C9_HUMAN	62	6
Pigment epithelium-derived factor	PEDF_HUMAN	46	5
Keratin, type I cytoskeletal 10	K1C10_HUMAN	59	4
Beta-2-glycoprotein 1	APOH_HUMAN	65	4
Complement C3	CO3_HUMAN	189	4
Metalloproteinase inhibitor 3	TIMP3_HUMAN	25	4
Fibulin-1	FBLN1_HUMAN	81	4
Gelsolin	GELS_HUMAN	86	3
Vimentin	VIME_HUMAN	54	3
60S acidic ribosomal protein P0-like	RLA0L_HUMAN	35	3
Serum amyloid P-component	SAMP_HUMAN	25	3

b

1	MKAAVLTLAV	LFLTGSQARH	FWQQDEPPQS	PWDRVKDLAT	VYVDVLKDSG
51	RDYVSQFKGS	ALGKQLNLKL	LDNWDSVTST	FSKLREQLGP	VTQEFWDNLE
101	KETEGLRQEM	SKDLEEVKAK	VQPYLDDFQK	KWQEEMELYR	QKVEPLRAEL
151	QEGARQKLHE	LQEKLSPLGE	EMRDRARAHV	DALRTHLAPY	SDELRQRLAA
201	RLEALKENGG	ARLAEYHAKA	TEHLSTLSEK	AKPALEDLRQ	GLLPVLESFK
251	VSFLSALEEY	TKKLNTQ			